Supporting Information

Nanocomposites of ionic copolymer integrating Gd-containing polyoxometalate as a multiple platform for enhanced MRI and pH-response chemotherapy

Tingting Zhou, Guofeng Wan, Bao Li* and Lixin Wu*

State Key Laboratory of Supramolecular Structure and Materials, College of Chemistry, Jilin University, Changchun, 130012, China

Corresponding Author E-mail: wulx@jlu.edu.cn; libao@jlu.edu.cn

Table of contents

1. Materials preparation 2
2. Cell and animal experiments 3
3. Structure analysis of CTPPA, BPMA and TMAPMA 6
4. Characterizations of PPMT and PPMT-POM nanocomposites 7
5. Drug release behavior 16
6. Quantitative analysis of DOX in cells 16
7. In vivo MRI 17
8. In vivo safety evaluation 21
9. Data for reference 21

1. Materials synthesis

Synthesis of chain transfer reagent 4-cyano-4-thiothiopropylsulfanyl pentanoic acid (CTPPA)

1-Propanethiol (7.50 g, 9.0 mL, 0.0985 mol) was slowly dropped into 250.0 mL of mixture of acetone and water (1:1 in volume ratio) containing potassium hydroxide (11.00 g, 0.196 mol). To the solution was added CS_2 (8.97 g, 0.118 mol) dropwise with stirring under an ice bath and the formed the reaction mixture was stirred at room temperature for another 2 h. Subsequently, *p*-tosyl chloride (22.50 g, 0.118 mol) dissolving in 62.5 mL of distilled acetone was added to above reaction system dropwise under vigorously stirring. After 1 h of reaction, the pH was adjusted to about 2 and then the solution was extracted with ethyl acetate, the organic phase was dried and evaporated over a rotary evaporator, giving the product bis(propylsulfanylthiocarbonyl) disulfide as a brown viscous liquid.

To 115.0 mL ethyl acetate were dissolved bis(propylsulfanylthiocarbonyl) disulfide (6.87 g, 22.75 mmol) and 4,4'-Azobis(4-cyanovaleric acid) (V501, 7.02 g, 25.07 mmol) and the solution was refluxed with stirring for 24 h. Afterwards, the solvent was evaporated under vacuum, and the crude product was purified by column chromatography using ethyl acetate/hexane (1/4, v/v) as eluent.

Synthesis of trimethyl ammonium bromide propyl-methacrylate (TMAPMA) monomer

As presented in Scheme S1, 3-bromo-1-propanol (15.37 g, 0.110 mol) and triethylamine (12.37 g, 17.0 mL, 0.122 mol) were added to 213.0 mL distilled dichloromethane in a three-necked flask equipped with a constant pressure drop funnel containing 12.0 mL methacryloyl chloride (12.96 g, 0.124 mol). The methacryloyl chloride in dropping funnel was dropped slowly into the dichloromethane solution in an ice bath. After the addition completed, the solution was stirred overnight at room temperature. The reaction was then quenched by adding 10.0 mL methanol under stirring for 30 min, and half of the solvent was removed by rotary evaporation. The rest of the organic phase was washed with saturated $NaHCO_3$ aqueous solution (1×70 mL) and water (2×70 mL), and dried over anhydrous magnesium sulfate. The raw product obtained from evaporation in vacuum was further purified by silica column chromatography with a mobile phase of ethyl acetate/hexane (1/50, v/v), giving a clear and colorless liquid 3-bromopropyl methacrylate.

The monomer TMAPMA was synthesized through a quaternization of the above product 3-bromopropyl methacrylate with trimethylamine. 3-bromopropyl methacrylate (0.75 g, 3.62 mmol) was dispersed in 5.0 mL ethanol in a single-neck round bottom flask, the flask was ended with a glass stopper as soon as trimethylamine methanol solution (33.0 wt%, 7.0 mL) was added in one batch under stirring at room temperature, and the seam of the flask was wrapped with Teflon tape to reduce the leakage of trimethylamine gas. During 5 days reaction time, additional 2.0 mL of trimethylamine methanol solution was added every two days. Finally, the solvent and unreacted trimethylamine were removed via rotary evaporation, and the obtained viscous liquid was precipitated into 20.0 mL of ice diethyl ether and kept in refrigerator maintained at about −20°C for 3 days, giving a white solid product after filtration.

Synthesis of macro-chain transfer reagent poly(polyethylene glycol methyl ether methacrylate)-based trithiocarbonate (macro-CTA PPEGMA)

As shown in Scheme S1, CTPPA (146.3 mg, 0.528 mmol), poly(ethylene glycol) methyl ether methacrylate (PEGMA, 3.956 g, 7.912 mmol) and initiator V501 (29.9 mg, 0.107 mmol) were dissolved in 4.0 mL

deionized water in a long-neck flask with the aid of sonication, and the solution was bubbled with nitrogen at room temperature 1 h, and then the reaction flask was immersed in a 70 ℃ oil bath. The polymerization was conducted at 70 ℃ in the dark for 9 h and then quenched by pouring into iced water, giving macro-CTA PPEGMA as a yellow fluid after following a dialysis and lyophilization.

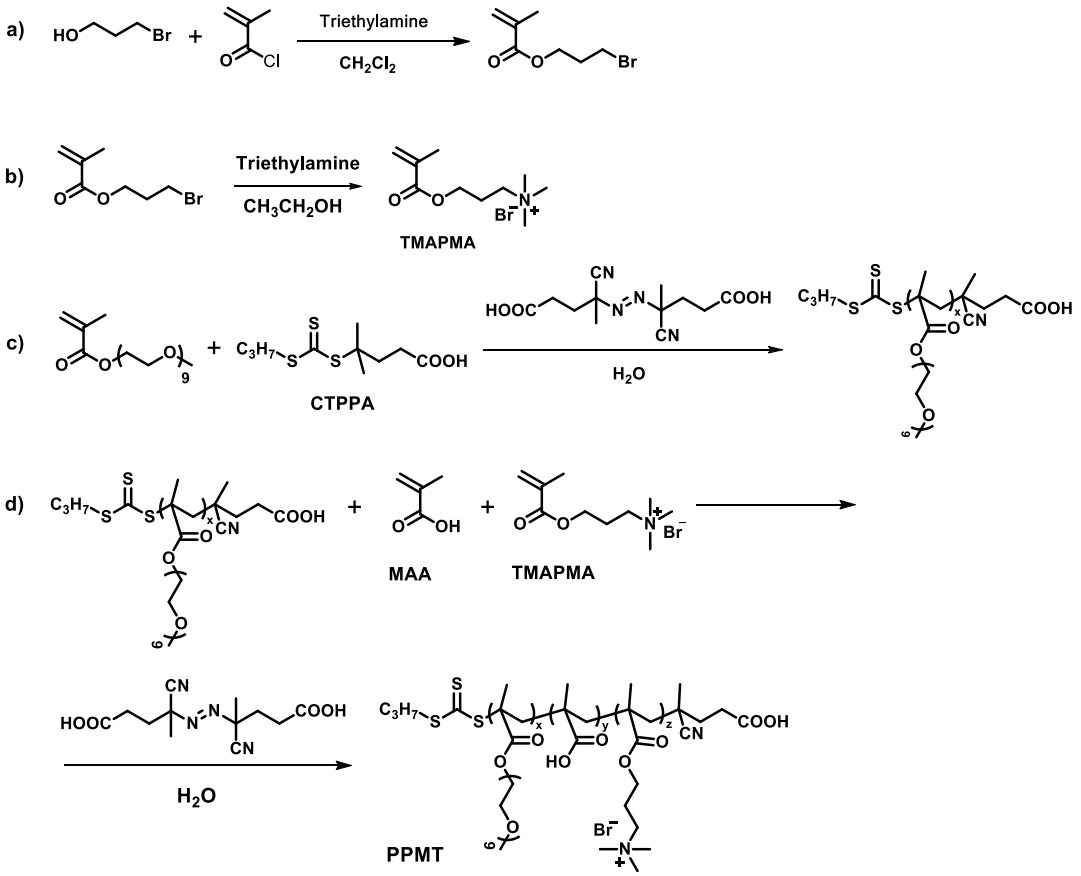

Scheme S1. Synthesis routes of monomer TMAPMA and block copolymer PPMT.

2. Cell and animal experiments

In vitro cytotoxicity

The biocompatibility of the nanocomposites and cytotoxic effect of DOX loaded $PPMT_2$-$GdSiW_{11}$ nanocomposites were both assessed via a MTT assay against HeLa cells. Briefly, HeLa cells were cultured in Dulbecco's modified eagle medium (DMEM) supplemented with high glucose, sodium carbonate, 10% fetal bovine serum, 1% penicillin and 1% streptomycin under 5% CO_2 at 37 °C. HeLa cells in a logarithmic growth phase were digested with trypsin, and then seeded in 96 well plates at a cell density of 3×10^3 per well in 100 μL DMEM medium. After incubation for 24 h at 37 °C in the incubator, the culture medium was replaced with total volume of 100 μL fresh culture medium containing 10 μL of $PPMT_2$-$GdSiW_{11}$ nanocomposites, $GdSiW_{11}$, DOX loaded $PPMT_2$-$GdSiW_{11}$ nanocomposites and free DOX solutions seperately at different concentrations from 0 to 100 μg mL^{-1}, and the incubation was continued for another 48 h. Subsequently, 20 μL of MTT solution (5 mg mL^{-1}) was added to each well, and the plate was further incubated for about 4 h. The medium containing free MTT was removed, and the MTT-formazan crystals

generated by living cells were dissolved by adding 150 μL of DMSO under oscillation. The absorbance of the above solution was measured by using a microplate reader at 490 nm. The cell viability data were presented as mean values of three measurements.

Cellular uptake study

Cellular uptake process of free DOX and DOX loaded nanocomposites was detected and evaluated by fluorescence microscope and flow cytometry. For immunofluorescence studies, HeLa cells were seeded onto cover slip in a six well plate at a cell density of 3×10^5 cells per well and incubated for 24 h to allow appropriate cell adhesion. The medium was substituted with fresh medium containing 10 μL of 6.35 μg mL^{-1} DOX·HCl or 50 μg mL^{-1} DOX loaded nanocomposites (6.35 μg mL^{-1} equivalent to DOX concentration), and the cells were cultivated for a certain time (0.635 μg mL^{-1} DOX for 24 h and 6.35 μg mL^{-1} DOX for 48 h) in the dark at 37 °C. Afterwards, the nutrient solution was removed, and the HeLa cells were washed three times with PBS to remove remaining DOX or DOX loaded nanocomposites. The HeLa cells were fixed in 4% phosphate-buffered paraformaldehyde for 30 min, and then the cell nuclei were stained with Hoechst 33342 for 15 min, following the manufacturer's instructions. The prepared sample on cover slip was observed by using a fluorescent microscope with excitations at 340 nm for Hoechst 33342 and 488 nm for DOX, which emissions at 460 nm and 595 nm respectively.

For the flow cytometry characterization, HeLa cells were planted in a 6 well culture plate at a density of 3×10^5 per well and cultured overnight. The HeLa cells were treated with the same concentration of DOX or DOX loaded nanocomposites as the same as the above immunofluorescence experiment for the same determined time. Thereafter, the growth medium was discarded, and the cells were successively washed twice with PBS, digested with trypsin and centrifuged at 1000 rpm for 5 min. After re-suspending the cells in 0.50 mL PBS, the DOX fluorescence of the samples with 1×10^5 cells at least was analyzed by using an Accuri C6 flow cytometer (Becton Dicknson Biosciences, CA, USA) with an excitation wavelength of 488 nm.

Flow cytometric analysis

To quantify the cytotoxic effects of DOX and DOX loaded nanocomposites by flow cytometry, HeLa cells were cultured and treated with DOX or DOX loaded nanocomposites as the flow cytometry study mentioned above, and the final re-suspended cells were stained by 5 μL of Annexin V-APC and 5 μL of 7-AAD (7-amino-actinomycin D) (Annexin V-APC/7-AAD apoptosis detection kit, KeyGEN Biotech, China) for 5 min at 4 °C in turn following the manufacturer's instructions. The apoptotic activities of each sample with fifty thousand cells were estimated by using an Accuri C6 flow cytometry, and the fluorescence emission signals were collected in FL-3 and FL 4 detecting channel.

Experimental animals and HeLa tumor xenograft models

SPF grade female nude mice (5 weeks old) weighing ~20 g were obtained from the Experimental Animal Center (Shanghai, China). All animal experiments were approved and performed in compliance with the guidelines of the Institutional Animal Care and Use Committee (IACUC) of Jilin University and Shanghai Rat&Mouse Bio tech Co. Ltd. The female mice were maintained under conventional aseptic conditions and bred with free access to water and food. The HeLa tumor models were generated by subcutaneously

injecting of 200 μL HeLa cell suspension with a cell density of 1×10^7 per millilitre into the right flank region of each nude mouse. The tumors were allowed to grow up to 50−100 mm^3 before in vivo MR imaging and other in vivo experimentations. The total tumor volume (V, mm^3) of the mice was calculated using the following formula: V = major axis × $(\text{minor axis})^2/2$. The major and minor axes of the growing tumors were measured by a caliper daily.

In vivo MR imaging

For in vivo MR imaging test at 0.5 T, the adopted parameters were set at TR=400 ms, TE=18.5 ms, slice width=3 mm, slices=9, and the number of averages=8. Female nude mice bearing HeLa tumor with similar weights (about 20 g) were used as animal models. The DOX loaded $PPMT_2$-$GdSiW_{11}$ solution (100 μL, 7.8 mg mL^{-1}) was intravenously injected into the anesthetized mouse through the tail vein, and the mouse was imaged in coronal section at different time intervals (15, 30, 60, 180, 240, and 330 min post-injection). In order to validate the contrast ability of the sample nanocomposites intuitively at tumor sites, another mouse was intratumorally injected with the same sample (100 μL), and the transverse T_1-weighted images were acquired before and after injection at 15 and 30 min.

For comparison, 100 μL of commercial gadopentetate dimeglumine (Gd-DTPA) solution (0.53 mg mL^{-1}) with the same gadolinium molar quantity as the above DOX loaded nanocomposites was intravenously injected into a mouse, and coronal T1-weighted images were obtained at 30, 60, 90 min post-injection. Then, larger amount of Gd-DTPA (100 μL, 7.8 mg mL^{-1}) was intravenously injected into the mouse and the coronal T_1-weighted images were obtained at 30, 60 min post-injection. Besides, the transverse images of another mouse were also collected before and after intratumoral injection for 15 and 30 min as contrast. It should be emphasized that the molar amount of Gd element in Gd-DTPA (100 μL, 7.8 mg mL^{-1}) used here was about 15-fold higher than that of DOX loaded nanocomposites used above.

In vivo tumor therapy efficacy

For the in vivo anticancer activity evaluation of DOX and DOX loaded nanocomposites, the female nude mice bearing HeLa tumors were randomly divided into five treatment groups and each group contained three mice. The injection treatment process was then initiated, and this day was assigned as day 0. Five gr**o**ups (n=3) of mice were administered with the following treatments: (1) PBS (100 μL, control group); (2) DOX loaded nanocomposites at concentration of 40.0 mg kg^{-1} (100 μL, 5.0 mg kg^{-1} of DOX equivalent dose); (3) DOX loaded nanocomposites at concentration of 8.0 mg kg^{-1} (100 μL, 1.0 mg kg^{-1} of DOX equivalent dose); (4) free DOX at 5.0 mg kg^{-1}; (5) free DOX at 1.0 mg kg^{-1}. The mice were injected intravenously five times via the tail veins on day 0, 3, 6, 9 and 12. Meanwhile, the tumor sizes, body weights and whole body pictures of mice with a highlight on tumor sites were also monitored every 3 days during the 15 days of treatments. The tumor inhibition experiment was stopped on the 16th day, the tumors, hearts, livers, spleens, lungs and kidneys of the mice were eventually dissected for flow cytometry and immunohistochemical analysis. The tumor tissues were weighted and pictured before slice preparation. The cell apoptosis of tumors were quantitatively characterized by flow cytometry and terminal deoxynucleotidyl transferase-mediateddUTP nick-end labeling (TUNEL) assay. For flow cytometry, part of the tumors were minced and digested with trypsin, followed by flow cytometry measurements as previously

described. Then, the tumor tissues and organs were fixed in 10% (v/v) formaldehyde for 2 days and then embedded in paraffin, and 4-7 μ m paraffin sections were prepared for the subsequent staining. After deparaffinization and rehydration, the tumor sections were treated with TUNEL, and diaminobenzene (DAB) was used for visualization and detection of deoxyribonucleic acid (DNA) fragmentation resulting from signals of apoptosis cell. The paraffin-embedded tumor tissues, hearts, livers, spleens, lungs and kidneys slices were stained with hematoxylin and eosin (H&E) for H&E analysis, and then observed by upright microscopy. All of the pictures were presented at 200×magnification.

3. Structure analysis of CTPPA, BPMA and TMAPMA

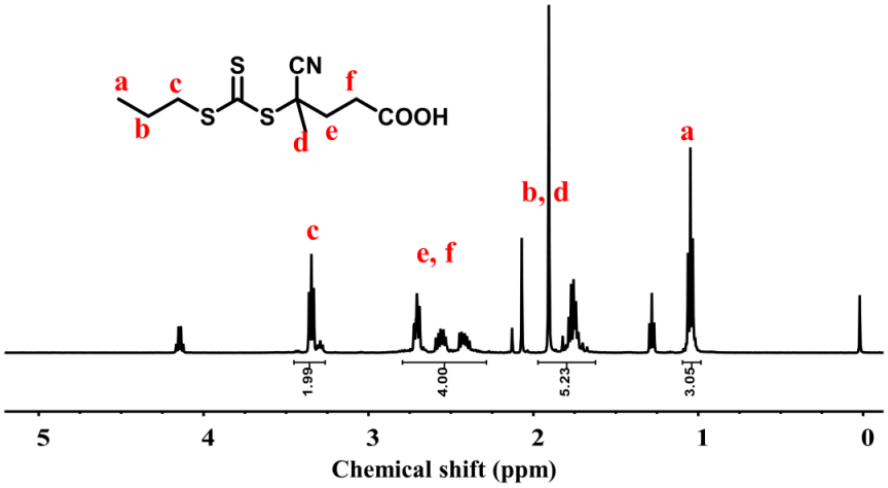

Fig. S1 500 MHz ^{1}H NMR spectrum of chain transfer agent CTPPA in $CDCl_3$. ^{1}H NMR ($CDCl_3$, 500 MHz) δ (ppm): 1.05 (3H, t, C*H*$_3$-CH$_2$), 1.67−1.93 (5H, m, CH$_3$–C*H*$_2$–CH$_2$– and C*H*$_3$), 2.37–2.77 (4H, m, HOOC–C*H*$_2$–C*H*$_2$–), 3.30 (2H, t, CH$_3$–CH$_2$–C*H*$_2$–)

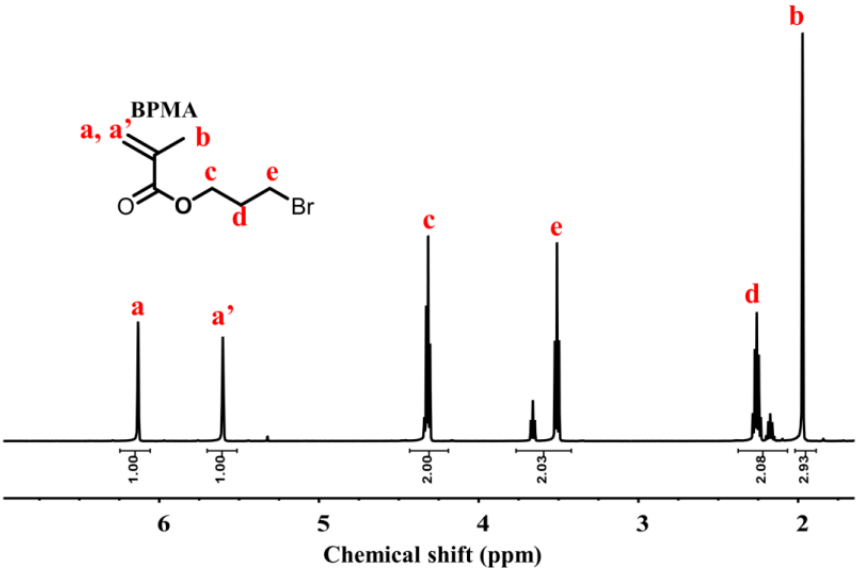

Fig. S2 500 MHz ^{1}H NMR spectrum of bromopropyl methyl methacrylate (BPMA) in $CDCl_3$. ^{1}H NMR ($CDCl_3$, 500 MHz) δ (ppm): 1.97 (3H, t, C*H*$_3$), 2.14−2.31 (2, m, Br–CH$_2$–C*H*$_2$–), 2.37–3.47−3.69 (2H, m, Br–C*H*$_2$–), 4.31 (2H, m,–O–C*H*$_2$–), 5.58−6.16 (2H, d, C*H*$_2$=C–).

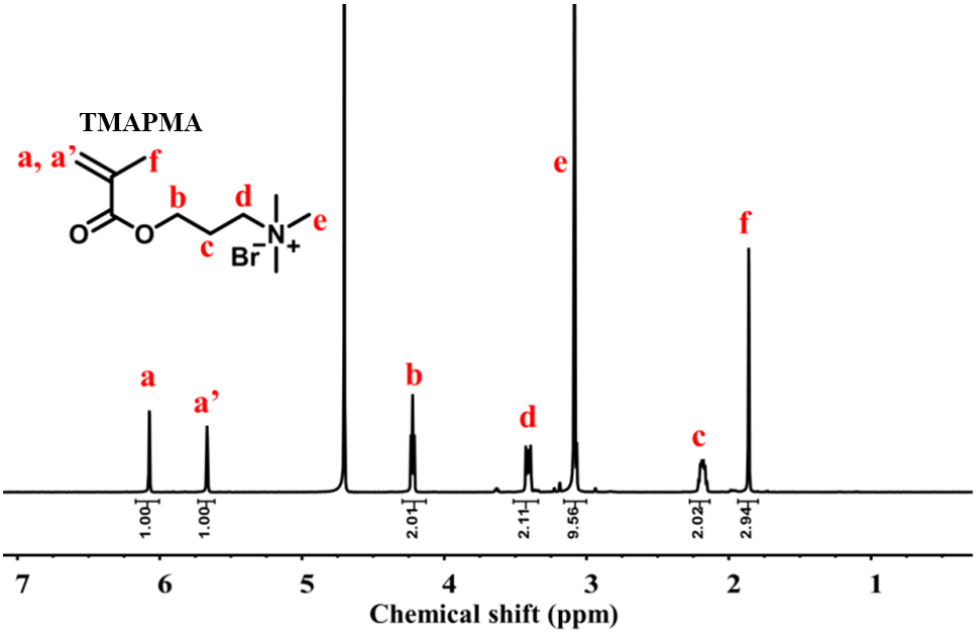

Fig. S3 500 MHz ^{1}H NMR spectrum of monomer TMAPMA in D_2O. ^{1}H NMR (D_2O, 500 MHz) δ (ppm): 1.86 (3H, t, C*H*$_3$), 2.19 (2, quint, –CH$_2$–C*H*$_2$–CH$_2$–), 3.08 (9H, s, –N–(C*H*$_3$)$_3$), 3.40 (2H, t,–N–C*H*$_2$–), 4.22 (2H, t,–O–C*H*$_2$–), 5.07−6.07 (2H, d, C*H*$_2$=C–).

4. Characterizations of PPMT and PPMT-polyoxometalates nanocomposites

Table S1. The recipes of PPMT block copolymer with different monomer ratios

Samples	V501 mg	Macro-CTA mg	MAA mg	TMAPMA mg	Water mL	Time h
PPMT$_1$	2.4	274.4	98.8	156	2.0	10
PPMT$_2$	1.38	96.2	55.4	147.1	2.0	10
PPMT$_3$	3.3	204.8	117.9	318.0	4.0	10
PPMT$_4$	1.52	96.8	55.2	150.4	2.0	10

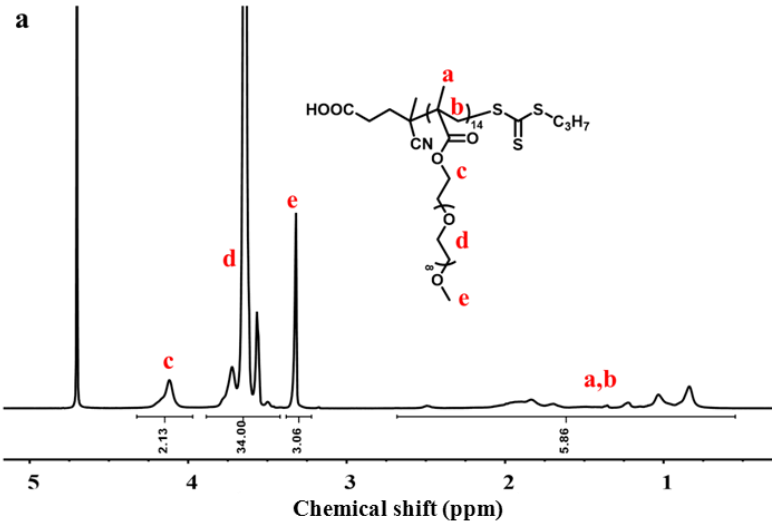

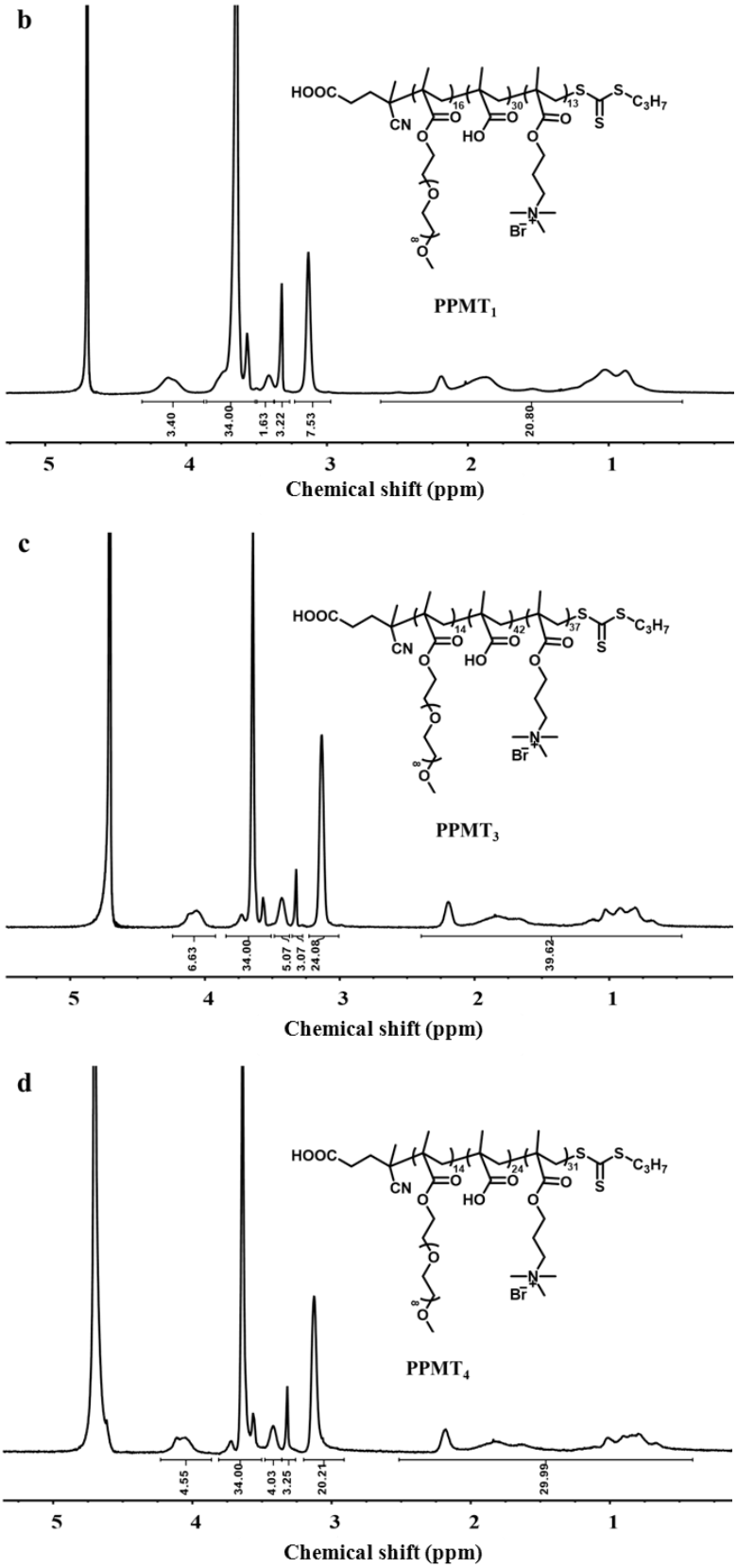

Fig. S4 ^{1}H NMR spectra of (a) macro-CTA PPEGMA, (b) $PPMT_1$, (c) $PPMT_3$ and (d) $PPMT_4$ in D_2O, and the unit number ratios of PEGMA, MAA and TMAPMA in $PPMT_1$, $PPMT_3$ and $PPMT_4$ were calculated to be 16:30:13, 14:42:37 and 14:23:31, respectively.

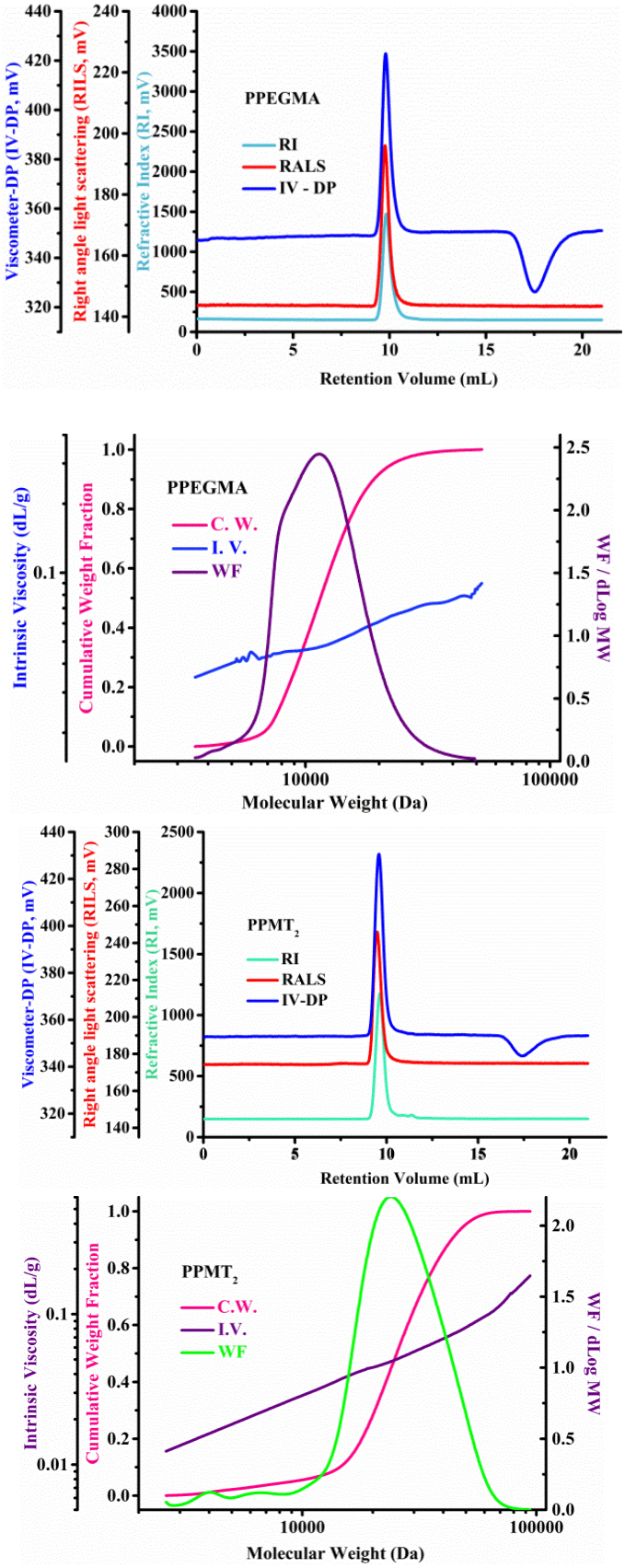

Fig. S5 The SEC results of PPEGMA and $PPMT_2$ aqueous solution with 0.1 M $NaNO_3$ as the eluent at the flow rate of 0.7 mL/min at 45 ℃.

Table S2. Summary of SEC results.

Sample name	M_n	M_w	M_z	M_p	M_w/M_n
PPEGMA	10954	12654	14914	12822	1.155
PPMT	20512	27139	32319	26830	1.323

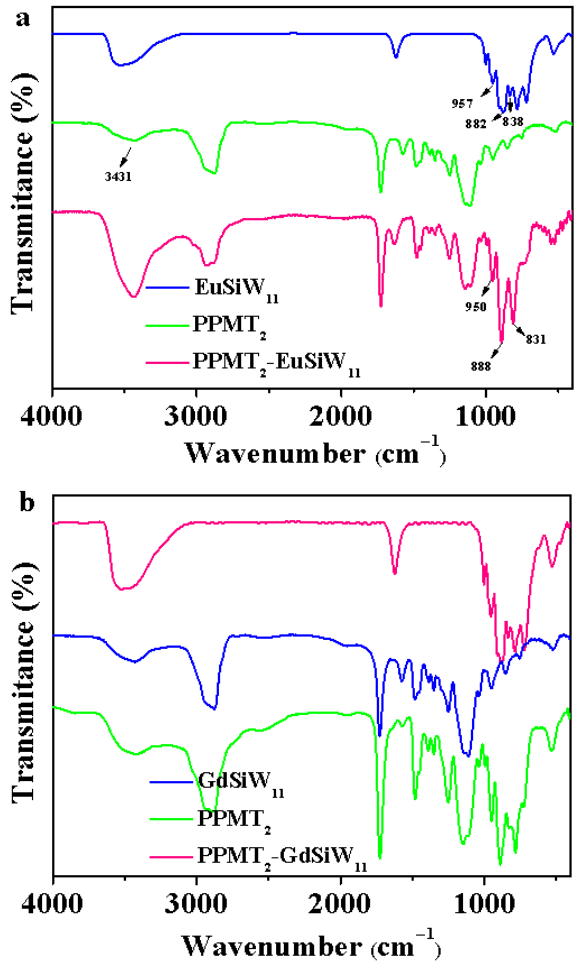

Fig. S6 FT-IR spectra of (a) $EuSiW_{11}$, $PPMT_2$ and $PPMT_2$-$EuSiW_{11}$ nanocomposites and (b) $GdSiW_{11}$, $PPMT_2$ and $PPMT_2$-$GdSiW_{11}$ nanocomposites.

Table S3. The elemental analysis results of polymer and the composites.

		N[%]	C[%]	H[%]	S[%]
PPEGMA	Calcd. ($C_{10}H_{15}O_2S_3N(C_{23}H_{44}O_{11})_{14.0}$, NMR, %)	0.18	55.18	8.8	1.24
	Calcd. ($C_{10}H_{15}O_2S_3N(C_{23}H_{44}O_{11})_{21.5}$, SEC, %)	0.13	55.32	8.84	0.88
	Found (%)	0.20	55.25	8.92	0.83
$PPMT_2$	Calcd. ($C_{10}H_{15}O_2S_3N(C_{23}H_{44}O_{11})_{14.0}(C_{10}H_{20}O_2NBr)_{24.0}(C_4H_6O_2)_{24.0}$, NMR, %)	2.23	51.15	8.06	0.61
	Calcd. ($C_{10}H_{15}O_2S_3N(C_{23}H_{44}O_{11})_{14.0}(C_{10}H_{20}O_2N)_{24.0}(C_4H_5O_2)_{24.0}(HBr)_{6.5}$, NMR, %)	2.45	56.23	8.74	0.67
	Calcd. ($C_{10}H_{15}O_2S_3N(C_{23}H_{44}O_{11})_{21.5}(C_{10}H_{20}O_2N)_{36.8}(C_4H_5O_2)_{36.8}(HBr)_{10}$, SEC, %)	2.43	56.31	8.76	0.44
	Found (%)	2.20	56.65	9.26	0.14
$PPMT_2$-$GdSiW_{11}$	Calcd. ($C_{10}H_{15}O_2S_3N(C_{23}H_{44}O_{11})_{14.0}(C_{10}H_{20}O_2N)_{24.0}(C_4H_5O_2)_{24.0}K_{12.4}(GdSi_2W_{22}O_{78})_{2.8}$, %)	1.18	27.06	4.18	0.32
	Found (%)	1.11	27.25	4.40	0.04

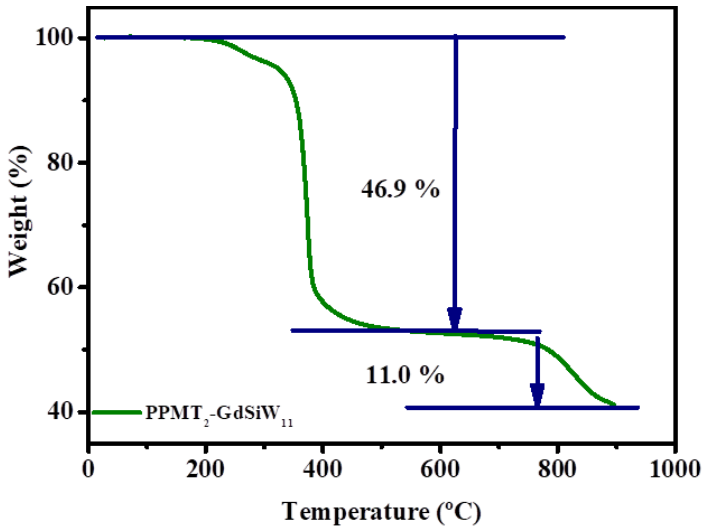

Fig. S7 Thermogravimetic analysis of $PPMT_2$-$GdSiW_{11}$ nanocomposites.

Table S4. The drug loading results of polyoxometalates and their composites.

Sample	DLC (%)	DLE (%)
EuW_{10}	32.8	97.6
$PPMT_1$-EuW_{10}	14.4	76.6
$PPMT_2$-EuW_{10}	19.0	67.1
$GdSiW_{11}$	21.1	95.2
$PPMT_1$	15.5	62.5
$PPMT_2$	15.6	62.7
$PPMT_1$-$GdSiW_{11}$	12.6	80.5
$PPMT_2$-$GdSiW_{11}$	12.7	96.7
$PPMT_3$-$GdSiW_{11}$	10.6	80.6
$PPMT_4$-$GdSiW_{11}$	11.2	94.8
$PPMT_3$-$P_8W_{48}V_{12}$	8.5	60.8
$PPMT_3$-Mo_{176}	9.4	95.5

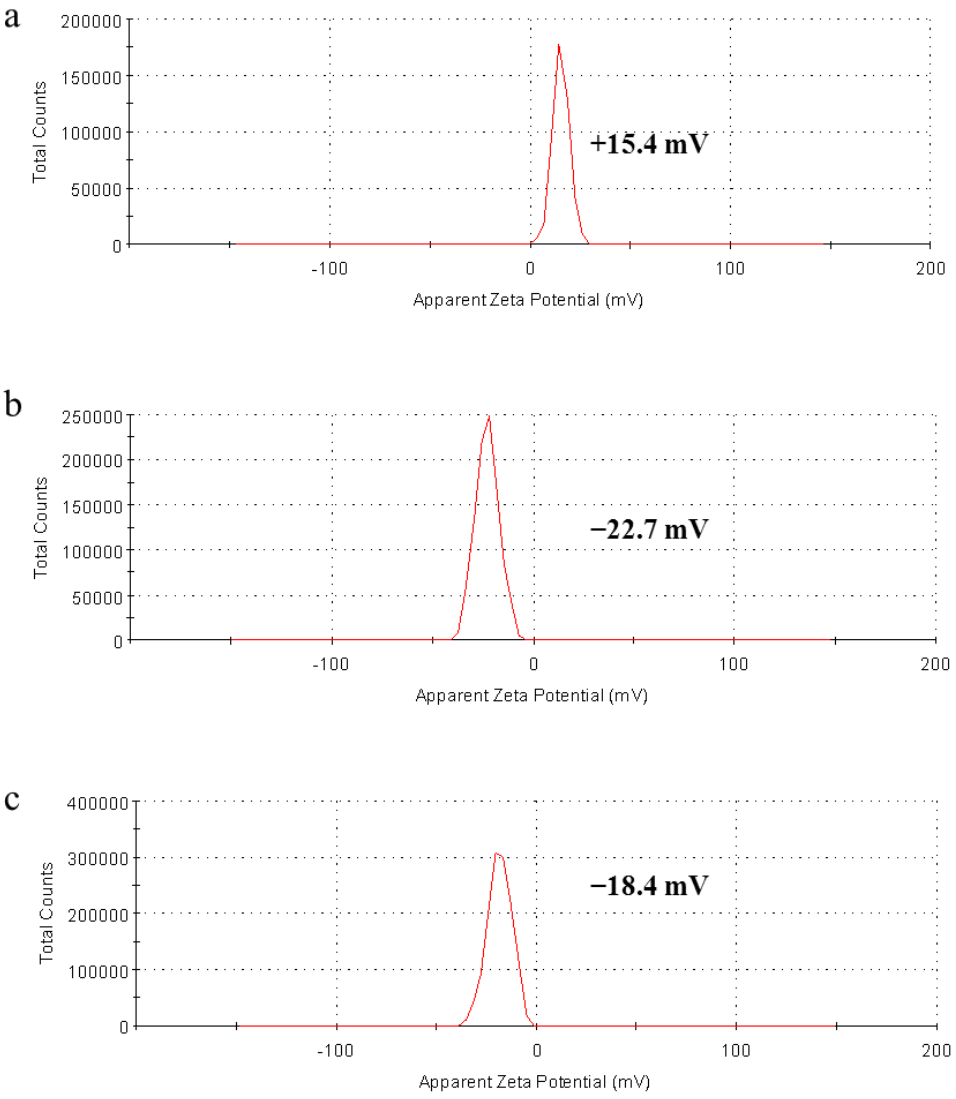

Fig. S8 Zeta potential results of (a) $PPMT_2$, (b) $PPMT_2$-$GdSiW_{11}$ nanocomposites and (c) DOX loaded $PPMT_2$-$GdSiW_{11}$ nanocomposites.

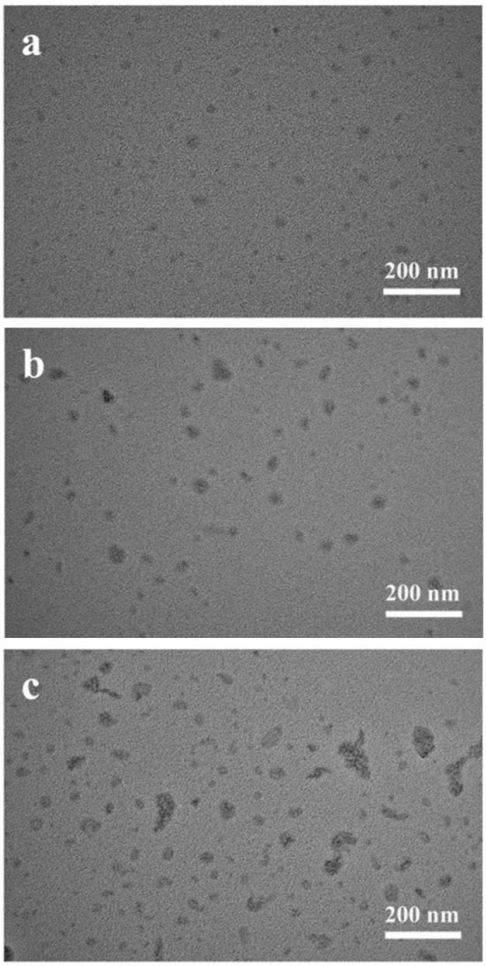

Fig. S9 TEM images of (a) $PPMT_1$-$EuSiW_{11}$, (b) $PPMT_3$-$EuSiW_{11}$ and (c) $PPMT_4$-$EuSiW_{11}$ nanocomposites.

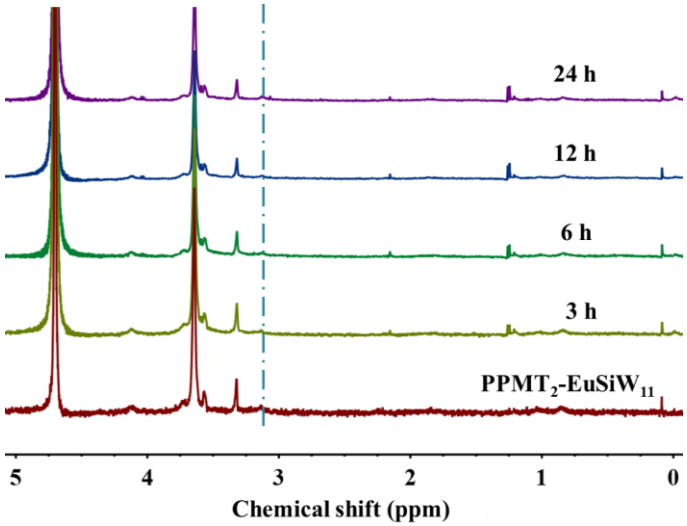

Fig. S10 ^1H NMR spectra of $PPMT_2$-$EuSiW_{11}$ nanocomposites in D_2O and 20 mM PBS solution after stirring for 3, 6, 12 and 24 h.

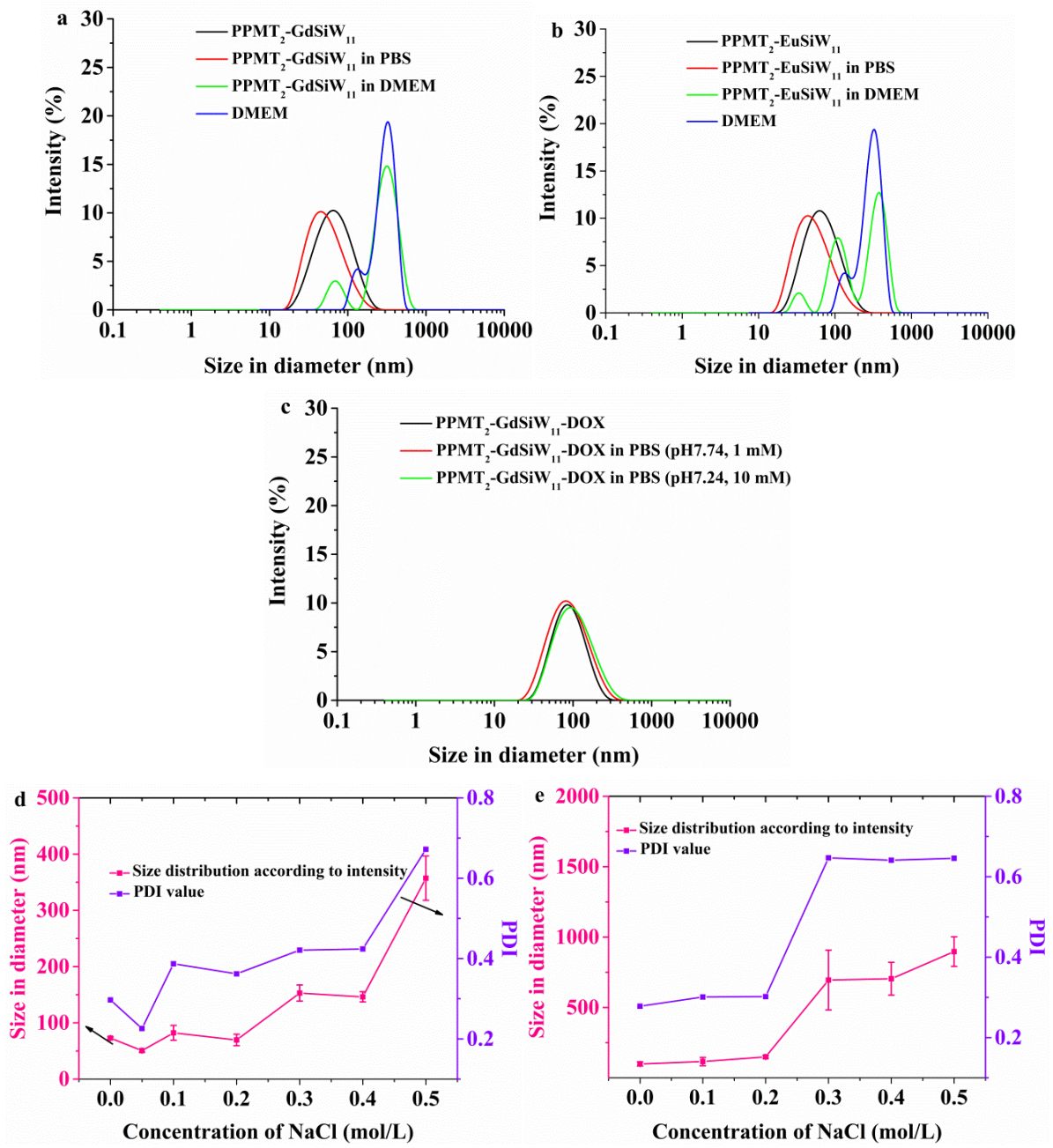

Fig. S11 Hydrodynamic size distributions of 0.05 mg mL^{-1} (a) $PPMT_2$-$GdSiW_{11}$ nanocomposites, (b) $PPMT_2$-$EuSiW_{11}$ nanocomposites and (c) DOX loaded $PPMT_2$-$GdSiW_{11}$ nanocomposites measured by DLS in various media such as water, PBS and DMEM, respectively. Plot of size and polydispersity dependence of (d) $PPMT_2$-$GdSiW_{11}$ nanocomposites and (e) DOX loaded $PPMT_2$-$GdSiW_{11}$ nanocomposites *versus* concentration of NaCl solution, where the concentration of the nanocomposites was set at 0.05 mg/mL.

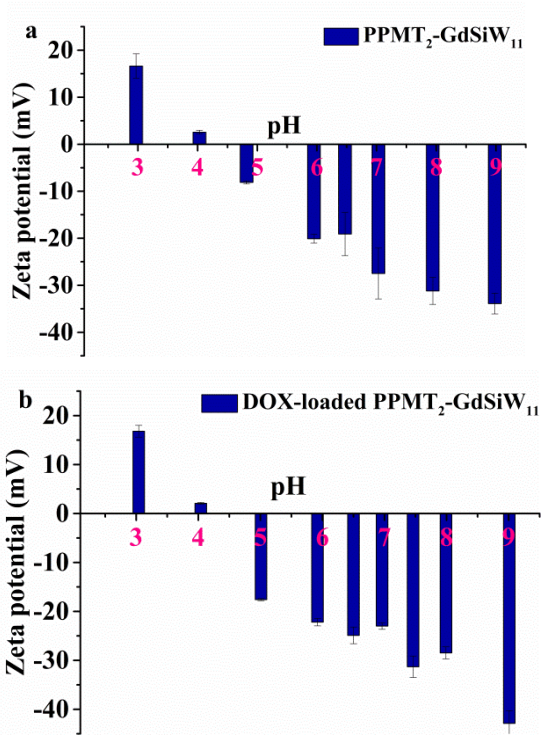

Fig. S12 Plot of pH dependent zeta potential variations of (a) $PPMT_2$-$GdSiW_{11}$ nanocomposites and (b) DOX loaded $PPMT_2$-$GdSiW_{11}$ nanocomposites.

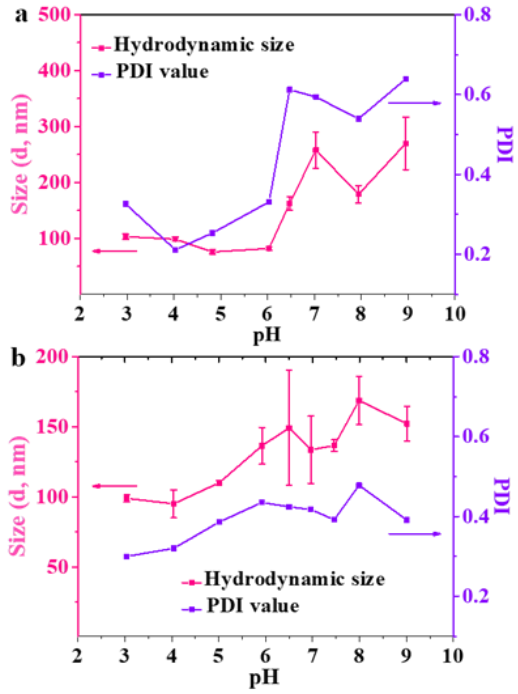

Fig. S13 Variation plots of hydrodynamic diameter (left axis) and polydispersity (right axis) versus the pH change of $PPMT_2$-$GdSiW_{11}$ nanocomposites without (a) and with (b) DOX loading at the concentration of 0.05 mg mL^{-1} in water

5. Drug release behavior

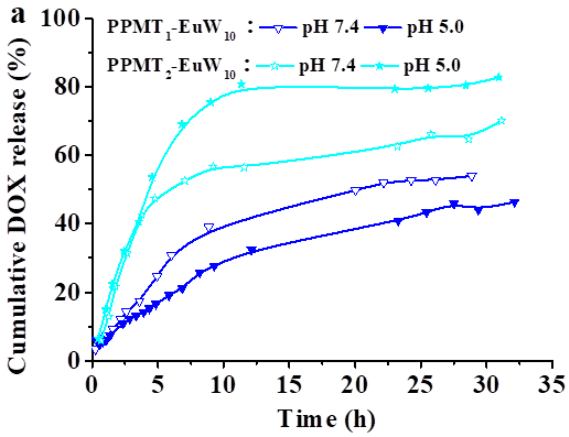

Fig. S14 Drug release profiles of DOX loaded PPMT-EuW_{10} nanocomposites.

6. Quantitative analysis of DOX in cells

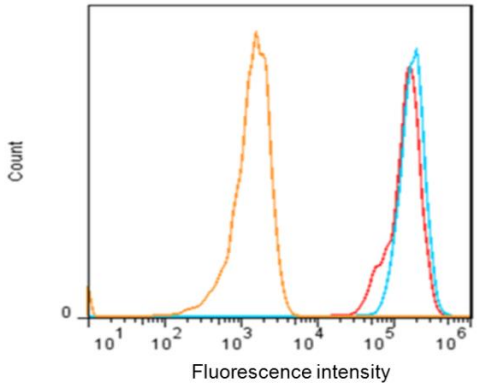

Fig. S15 Cell uptake count of blank control (orange line), free DOX (red line) and DOX loaded $PPMT_2$-$GdSiW_{11}$ nanocomposite (blue line) with equivalent DOX dose of 6.35 μg mL^{-1} after incubation in HeLa cells for 48 h from flow cytometry.

7. In vivo MRI

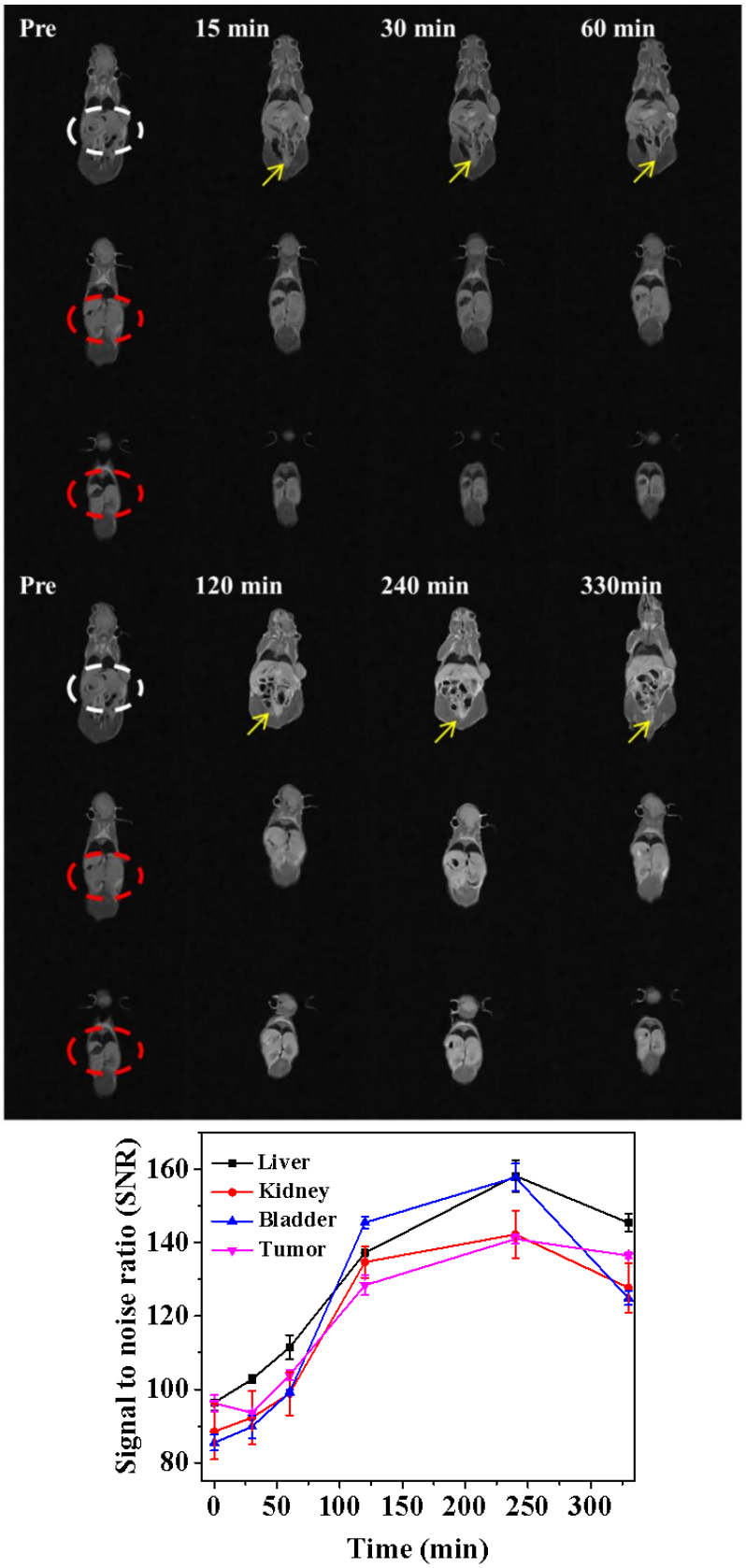

Fig. S16 Coronal T_1-weighted MR images (top) centered on liver (white circle), bladder (yellow arrow) and kidney (red circle region) of mice before and after intravenous injection of DOX loaded nanocomposites aqueous solution (100 μL, 7.8 mg mL^{-1}) for 15, 30, 60, 120, 240, and 330 min, and the corresponding MR signal to noise ratio (bottom) in tumor and organs versus time after intravenous injection.

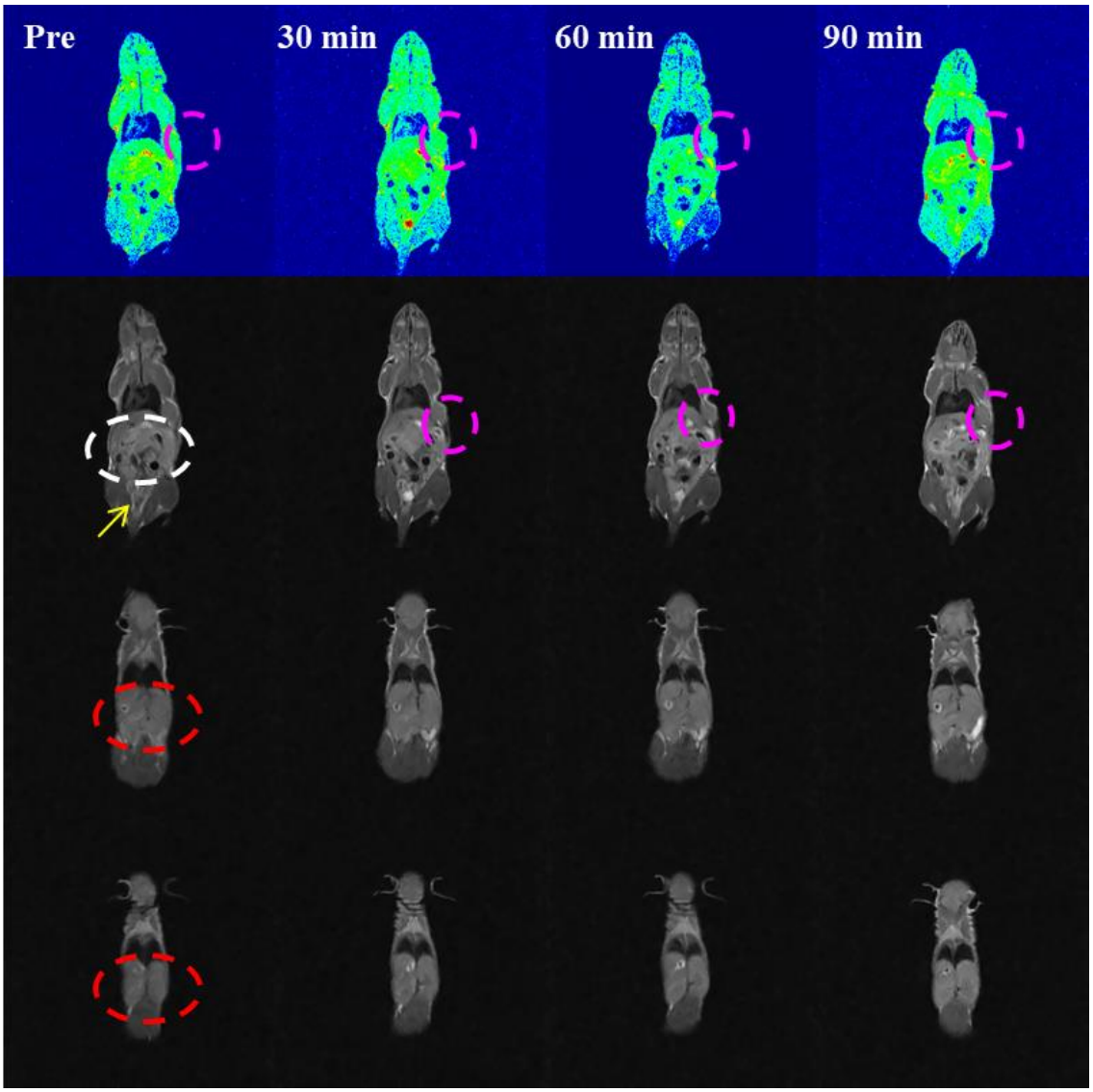

Fig. S17 Coronal T_1-weighted MR images centered on tumor site (pink circle), liver (white circle), bladder (yellow arrow) and kidney (red circle region) of mice before and after intravenous injection of commercial contrast agent Gd-DTPA aqueous solution (100 μL, 0.53 mg mL^{-1}) for 30, 60 and 90 min.

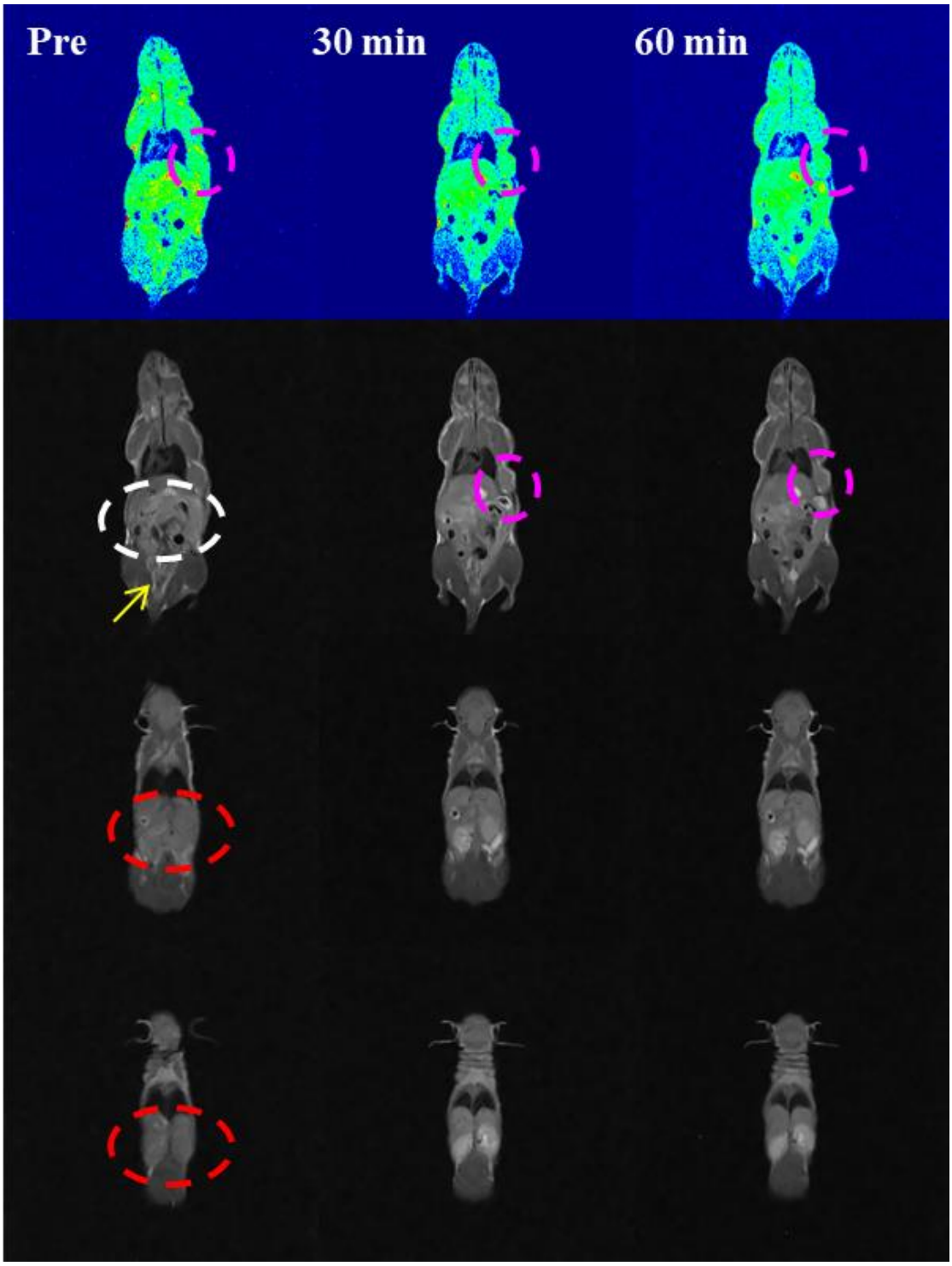

Fig. S18 Coronal T_1-weighted MR images centered on tumor site (pink circle), liver (white circle), bladder (yellow arrow) and kidney (red circle region) of mice before and after intravenous injection of commercial contrast agent Gd-DTPA aqueous solution (100 μL, 7.8 mg mL^{-1}) for 30 and 60 min.

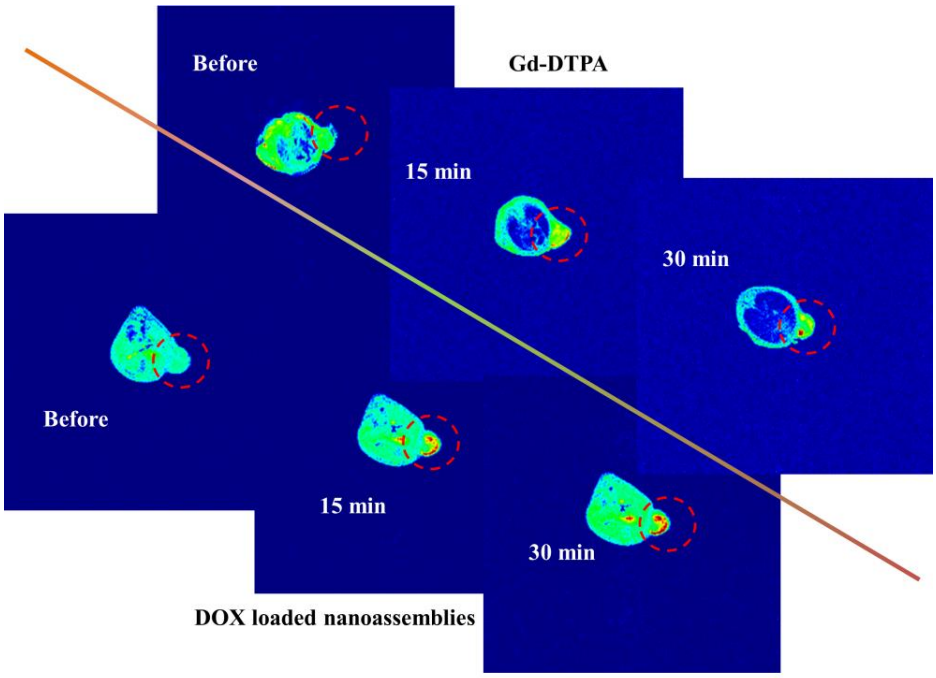

Fig. S19 Transverse T_1-weighted MR images of mice before and after intratumoral injection of DOX loaded $PPMT_2$-$GdSiW_{11}$ nanocomposites and Gd-DTPA aqueous solution (100 μL, 7.8 mg mL^{-1}) respectively for 15 and 30 min, the red circle region indicated the tumor region.

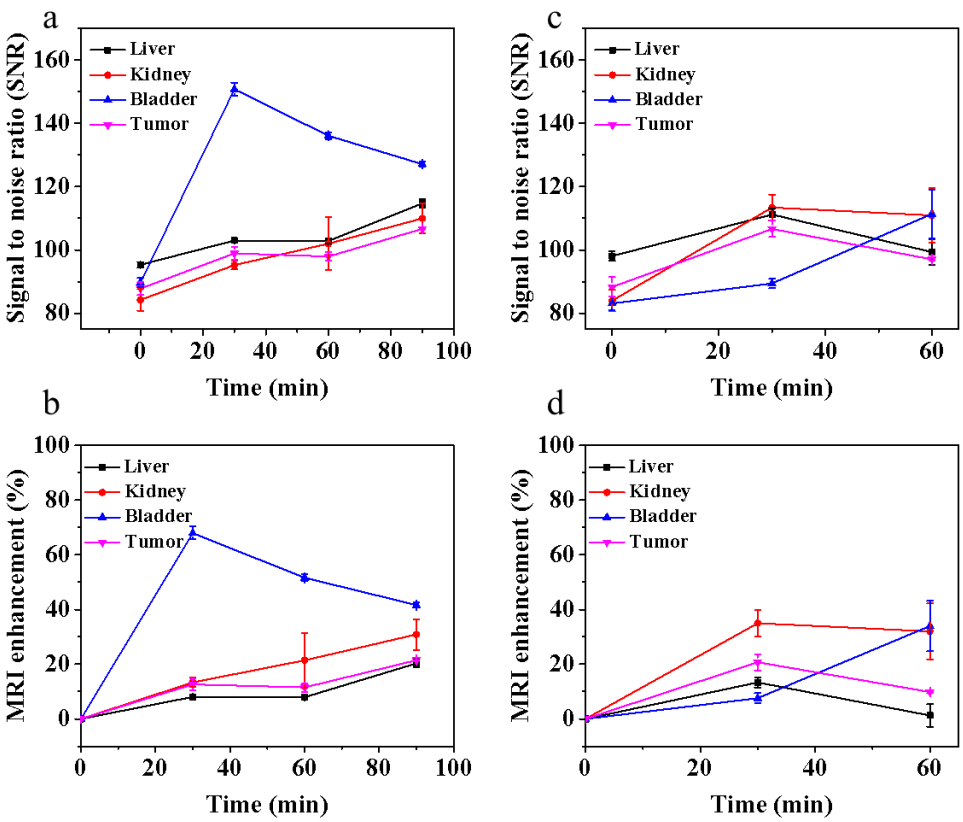

Fig. S20 Signal to noise ratio SNR and MRI enhancement of the region of interests in mice with respect to (a, b) low dose Gd-DTPA injection and (c, d) high dose Gd-DTPA injection at different time intervals, respectively. The SNR value was extracted from the original black-and-white T_1-weighted MRI profiles in Figure S17 and S18.

8. In vivo safety evaluation

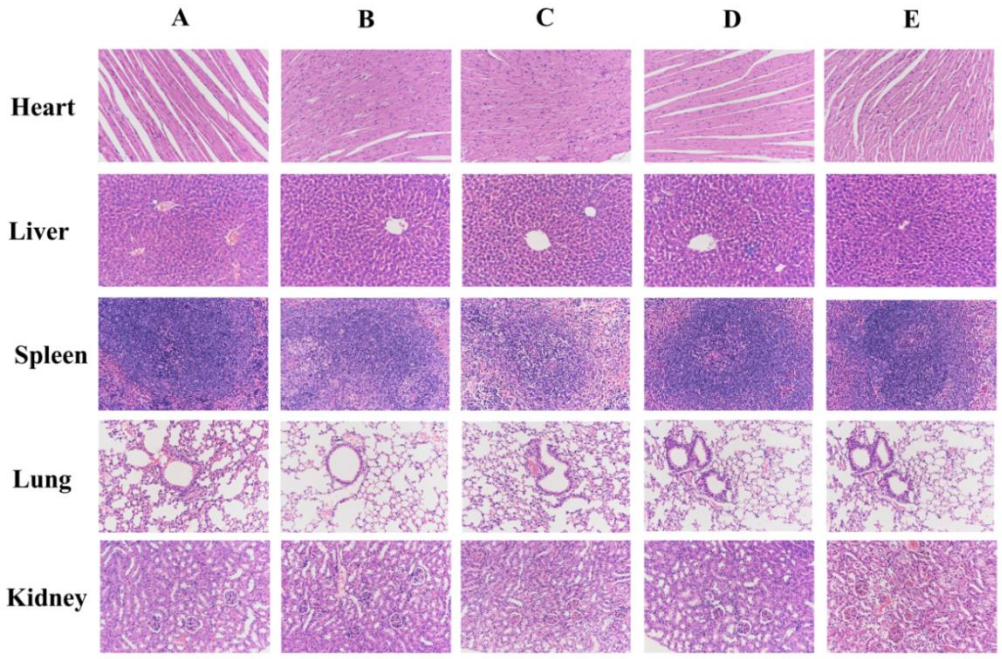

Fig. S21 The H&E staining results of histological assays of hearts, livers, spleens, lungs and kidneys dissected from mice on day 16 (200×magnification) : (A) PBS; (B) DOX-loaded nanocomposites (5 mg kg^{-1}); (C) DOX-loaded nanocomposites (1 mg kg^{-1}); (D) Free DOX (5 mg kg^{-1}); (E) Free DOX (1 mg kg^{-1}).

9. Data for reference

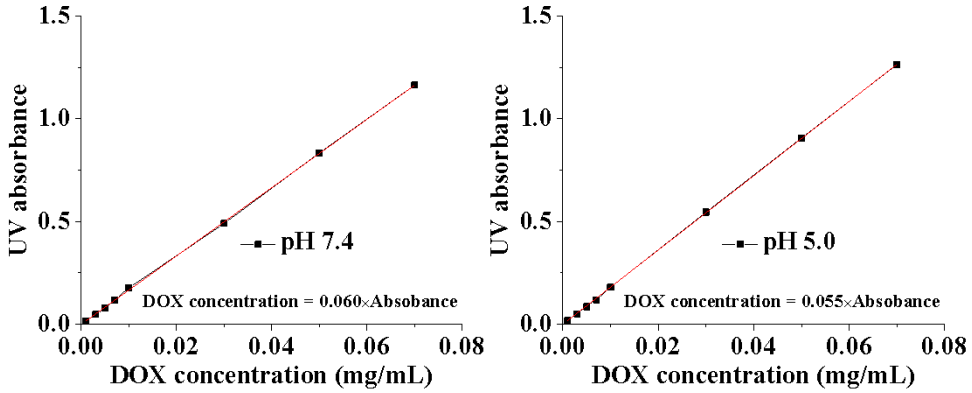

Fig. S22 Standard UV curve of DOX.

Table S5. The charge moles of each composition during drug loading.

Sample	TMAPMA/μM	Negative charge/μM	DOX/μM	Charge ratio
EuW_{10}	-	62.9	16.7	26.6%
$GdSiW_{11}$	-	22.6	5.2	23.0%
$PPMT_2$-$GdSiW_{11}$	22.0	29.2	6.6	
$PPMT_3$-$GdSiW_{11}$	14.8	17.5	4.1	
$PPMT_3$-$P_8W_{48}V_{12}$	15.6	16.8	4.6	
$PPMT_3$-Mo_{176}	14.6	16.6	4.6	

The charge ration referred to the ratio of negative charge of polyoxometalates to DOX. For the DOX loaded $PPMT_2$-$GdSiW_{11}$ nanocomposites, 7.3 molecules of DOX were loaded into the nanocomposites on a polymer molecule of $PPMT_2$ basis.